Postprint of: Woloszyk K., Garbatov Y., An enhanced method in predicting tensile behaviour of corroded thick steel plate specimens by using random field approach, Ocean Engineering, Vol. 213 (2020), 107803, DOI: 10.1016/j.oceaneng.2020.107803

An enhanced method in predicting tensile behaviour of corroded thick steel plate specimens by using random field approach

Krzysztof Woloszyk[a], Yordan Garbatov[b, 1]

[a] *Faculty of Ocean Engineering and Ship Technology, Gdansk University of Technology, G. Narutowicza 11/12 st., 80-233 Gdansk, Poland*

[b] *Centre for Marine Technology and Ocean Engineering (CENTEC), Instituto Superior Técnico, Universidade de Lisboa, Avenida Rovisco Pais 1049-001 Lisboa, Portugal*

Abstract

The present work investigates the possibility of using random field techniques in modelling the mechanical behaviour of corroded thick steel plate specimens. The nonlinear Finite Element method, employing the explicit dynamic solver, is used to analyse the mechanical properties of typical specimens. A material model considering full nonlinearity is used to evaluate the stress-strain response. The influence of major governing parameters of both specimen dimensions and random field is investigated through the sensitivity analysis. In order to validate the proposed methodology, results are compared with available experimental data showing an excellent agreement in both mechanical properties and stress-strain relationships. Additionally, the conclusion is made that the irregularities in the corroded surface are the main factor resulting in the decrease of mechanical properties. In this way, random field modelling appeared to be a practical and fast technique for modelling the corroded surfaces of steel structures in analysing their structural behaviour.

Keywords: Corrosion, Mechanical Properties, Finite Element Method, Random Field

1. Introduction

All metal structures operating in atmospheric or marine conditions are subjected to corrosion degradation (Garbatov et al., 2006), which leads to a thickness reduction. Nowadays, different models to evaluate the corrosion loss as a function of time exist (Garbatov et al., 2006; Melchers, 2008; Paik et al., 2004). Nevertheless, it is noticed that the mechanical properties of structural elements could be reduced with the corrosion degradation progress (Garbatov et al., 2014b). The combination of these two factors can severely reduce the strength of structures (Garbatov et al., 2014a; Saad-Eldeen et al., 2012; Wang et al., 2014; Woloszyk et al., 2018; Woloszyk and Garbatov, 2019a).

In recent years, different studies focused on the investigation, experimentally and numerically, of the mechanical properties reduction of steel specimens caused by corrosion degradation. The experimental analysis of corroded steel bars in natural and laboratory environment was conducted in (Fernandez and Berrocal, 2019; Kashani et al., 2013; Zhang et al., 2006). The maximum reduction in the case of yield strength was up to 30 % and 80 % in the case of total elongation for the most severely corroded elements. The measurements of the corrosion morphology shown that the minimum cross-sectional area may govern the mechanical properties reduction.

When analysing ship and offshore structures, the plates are more often used in their construction, and thus the flat specimens are used in defining the mechanical properties, and with this respect, many specimens of different levels of severity were analysed in (Garbatov et al., 2014b). For the specimens

[1] Corresponding author e-mail: yordan.garbatov@tecnico.ulisboa.pt; Telf (351) 21 841 7907

with corrosion severity above 20 %, the reduction of mechanical properties revealed to be very significant. The reduction is observed in all mechanical properties, i.e. yield stress, ultimate stress, Young modulus and total elongation. Other studies related to flat specimens were done in (Nie et al., 2019; Qin et al., 2016; Wang et al., 2017; Xu et al., 2019b, 2019a) leading to similar conclusions. Nevertheless, even for the lower level of corrosion degradation, the decrease of mechanical properties was also observed. The reduction was even magnified when the specimens were pre-stressed and corroded (L. Li et al., 2018; Li et al., 2019).

The majority of the studies agreed that ideally, uniform corrosion degradation would not cause a significant reduction of mechanical properties. In this way, the decrease is mostly caused by the non-uniformity of the corroded surface (Cairns et al., 2005; Du et al., 2005a, 2005b; Palsson and Mirza, 2002). This hypothesis is supported by (Garbatov et al., 2018), where specimens subjected to different cleaning methods, compared to only corroded ones, revealed to have higher values of the mechanical properties. In the case of the ship and offshore structures, the most common type of corrosion is the non-uniform one, and the above foundlings cannot be neglected.

Different mathematical models for predicting the mechanical properties of structural members were developed recently (Ahmmad and Sumi, 2010; Appuhamy et al., 2011; Fernandez et al., 2016; Flaks, 1978; Moreno et al., 2014; Nakai et al., 2004). Mostly they are based on the experimental results. A simplified model for corroded bars was shown in (D. Li et al., 2018). The model for corroded flat specimens was also developed in (Garbatov et al., 2014b). In the study performed by (Wang et al., 2017), the experimental results were compared with the FE estimations, and the agreement was excellent. Additionally, they showed that the results of different mathematical models might differ significantly. Thus, the unified approach to model the mechanical properties changes concerning corrosion needs to be developed.

The corrode plate surface, similar to a different natural phenomenon such as waves is stochastically originated. In this way, the modelling with the use of the random field (Jankowski and Walukiewicz, 1997) seems to be accurate for the purpose. The examples of engineering applications with the use of random field modelling may be found in (Górski et al., 2015; Górski and Winkelmann, 2017; Teixeira and Guedes Soares, 2008). The possibility of random techniques usage in corrosion modelling was shown in (Garbatov and Guedes Soares, 2017). Nevertheless, the stochastic modelling provides many samples which may need a large amount of computational time but may provide a good statistical base for the reliability analysis (Melchers, 2017; Woloszyk and Garbatov, 2019b) of the ship and offshore structures.

The present study is a continuation of the work done in (Woloszyk and Garbatov, 2020). In the previous study, the capabilities of random field modelling of corroded specimens were explored in the case of very thin specimens (1 mm of the initial thickness). The results were compared with the experimental data as presented in (Nie et al., 2019), and the evident agreement was observed for the lower level of the Degree of Degradation. However, for severely corroded plates, more significant deviations were observed. Nevertheless, the very thin plates can be found rarely in case of the ship and offshore structures. Thus, the present work explores the possibility of the random field modelling of corroded specimens of thicker thicknesses (in the range between 6 up to 9 mm). The nonlinear FE analysis performed with the use of the explicit dynamic solver is employed here. The sensitivity of the governing geometrical parameters of the specimen and random field is also analysed. The results are validated with experimental data provided in (Wang et al., 2017).

2. Corrosion modelling using random field approach

The random field, which is the set of spatially correlated random variables, seems to be the most suitable technique to model corroded plate surfaces. In the case of numerical modelling, the discretised random field needs to be used, where one of those discretisation methods may be found in (Ghanem and Spanos, 1991; Li and Der Kiureghian, 1993). In the current study, the Karhunen – Loeve expansion (Ghanem and Spanos, 1991) is employed. The Gaussian random field is defined by its mean $\mu(\boldsymbol{x})$, variance $\sigma^2(\boldsymbol{x})$ and autocovariance function $C(\boldsymbol{x},\boldsymbol{x}')$. The detailed explanation of random field was already presented in (Woloszyk and Garbatov, 2020). The square exponential autocovariance used in this study:

$$C(\boldsymbol{x},\boldsymbol{x}') = \exp\left(\frac{(\boldsymbol{x}-\boldsymbol{x}')^2}{c_0^2}\right) \tag{1}$$

where $(\boldsymbol{x}-\boldsymbol{x}')$ is the absolute distance between any two points in the meshed surface and c_0 is the correlation length. The spatial variation of the field is mostly dependent on the correlation length. With the increase of correlation length, the field becomes smoother, whereas, with the decrease of correlation length, the field became more irregular. Two fields with the same mean value and variance, but with different correlation lengths are presented in Figure 1.

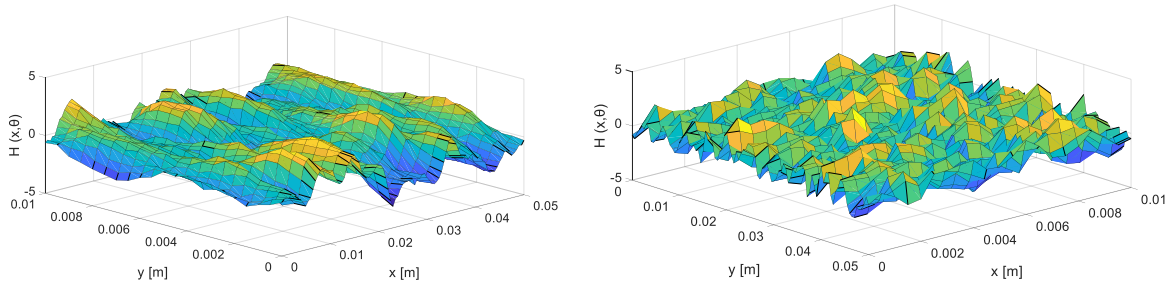

Figure 1. Strongly (left) and weakly (right) correlated field.

The MatLab software (Mathworks, 2019) with a specially developed program code (Constantine, 2012) is used to generate the Gaussian random field ($H(\boldsymbol{x})$) for the specified mesh and various correlation lengths. However, based on the measurements of corroded surfaces (Wang et al., 2017), it can be noticed that the maximum corrosion depth is often much higher than the mean value. This leads to the log-normal distribution, which is obtained by the transformation of the normal field:

$$L(\boldsymbol{x}) = \exp\big(\mu + \sigma H(\boldsymbol{x})\big) \tag{2}$$

where μ and σ are the location and scale parameters of the log-normal field, respectively. There need to be calibrated to produce a proper mean value and standard deviation of the currently developed field.

The random field can be generated for the assumed values of the mean value and standard deviation of the corrosion depth. However, in the present study, the statistical descriptors are calibrated based on the experimental results (Wang et al., 2017) to show the feasibility of the proposed methodology. The considered random field is assumed to be isotropic, whereas in real corrosion conditions some anisotropy is possible. However, for small-scale specimens, it could be observed that the corrosion surfaces are somewhat regular.

3. Finite Element modelling

For the simulation of the tensile test of steel specimens, ANSYS LS-DYNA (ANSYS Inc., 2019) software is employed. The multilinear stress-strain relationship of the material and SOLID 164 elements are used

with the explicit dynamics solver. Apart from the quasi-static origin of the tensile testing, the explicit solver is used to pass the convergence problem (Bäker, 2018), which originates from both corrosion degradation and necking phenomenon. In the standards of tensile testing (ISO, 2009), the engineering stress-strain curve is established. However, in the FE analysis, one needs to define the true stress-strain ($\sigma_{true} - \varepsilon_{true}$) relationship as:

$$\varepsilon_{true} = \ln(1 + \varepsilon) \tag{3}$$

$$\sigma_{true} = \sigma(1 + \varepsilon) \tag{4}$$

where σ and ε are engineering stress and strain, respectively.

The above formulations are valid up to the ultimate tensile strength point. Where the necking phenomenon starts to occur, and the power-law based procedure is introduced (Kwesi Nutor, 2017):

$$\sigma_{true} = K\varepsilon_{true}^{n} \tag{5}$$

where n and K are the strain hardening parameter and strength coefficient, respectively.

Figure 2 shows the specimen scheme and the FE model. The area of the corroded part of the specimen has a size of 50x25 mm, and thus the mesh is very dense in this region. In the case of mounting and transitional parts of the specimen, their finite-element size is not relevant, since there are mainly distributing the longitudinal load. To simulate the experimental conditions, the mounting parts are fixed, and one of them is subjected to a longitudinal displacement. The displacement is realised via small increments in the time domain in the explicit solver.

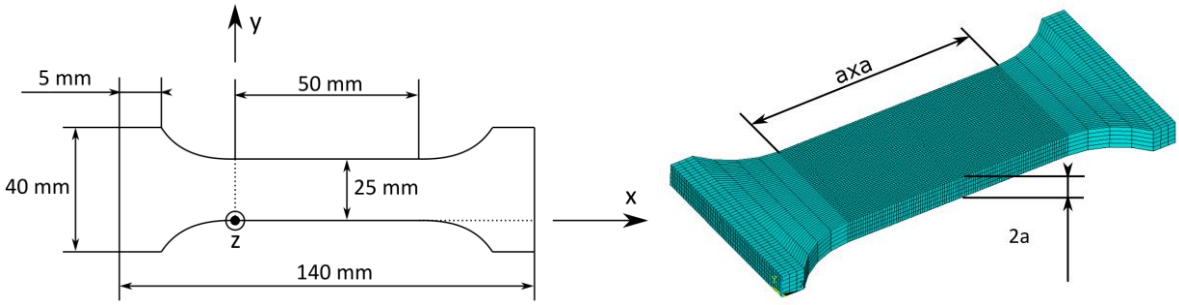

Figure 2. Specimen scheme (left) and FE model (right).

For identifying the proper element size, the mesh convergence studies are carried out. The results of the analysis with an element size, a from 0.5 mm up to 5 mm are presented in Figure 3. The most refined mesh provides accurate results. However, with the element size of 1 mm, the results are also accurate. Nevertheless, further analysis showed that the 0.5 mm mesh size should be chosen to provide a good representation of the corrosion field, especially for the weaker correlations. It is essential to mention that significant differences in total elongation between coarse and refined mesh reaching 40 % in case of 5 mm mesh are observed, which may be as a result of the complexity of the necking behaviour. During necking, the strain is highly non-uniform within the mid-cross-section, and the highest strain is visible in the middle. In FE modelling, only the strain in the middle of any particular element can be captured. When the element size is relatively big, the strain distribution is reasonably accurate, and the middle elements show smaller strain with comparison to the accurate one. Thus, the failure criteria are defined with a higher mean elongation, and the total elongation is higher when compared to an accurate one. With the mesh refinement, the total elongation tends to an accurate value.

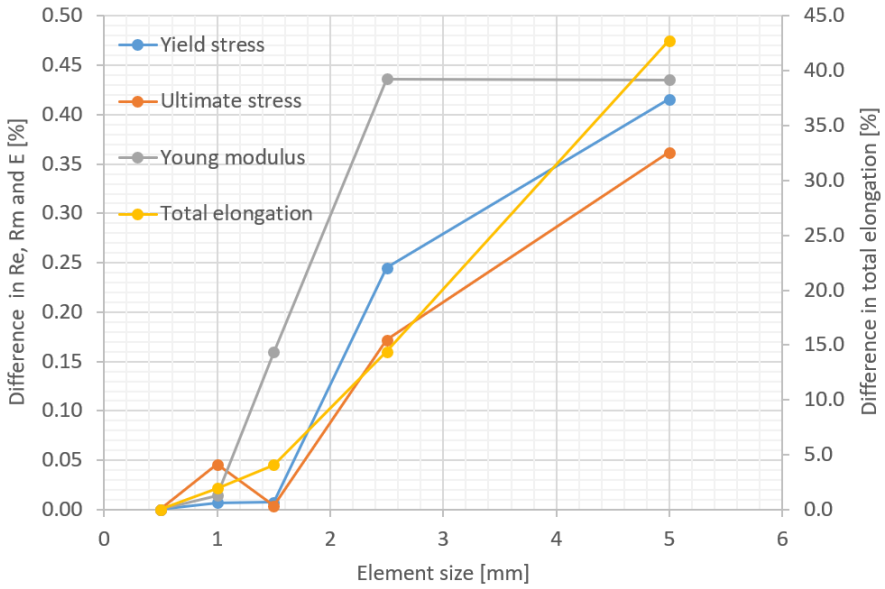

Figure 3. Mesh convergence studies.

The experimental results of (Wang et al., 2017) are used as a validation case, and the stress-strain curve from this study is taken as a basic one in the present study. The material properties of mild steel S235 are as follows: yield stress $Re = 292.6\ MPa$, Young modulus $E = 207\ GPa$, ultimate tensile stress $R_u = 435\ MPa$ and total elongation $\delta = 35.2\ \%$. The output engineering stress-strain curve and input curve for the FE analysis with a comparison to experimental one are presented in Figure 4. Both numerical and experimental curves are almost identical with a minimal deviation. The first part of the input curve was obtained using Eqns 3 and 4 up to the ultimate tensile stress point (strain equal to 0.182). The calibration of the second part is done using Eqn 5 and the following parameters: $\varepsilon_{failure} = 0.9\ [-], K = 750\ MPa, n = 0.214\ [-]$. The element breaks, when the defined failure strain is obtained. The proper modelling of the tensile behaviour in the FE analyses may be seen in Figure 5, where the necking phenomenon is visible.

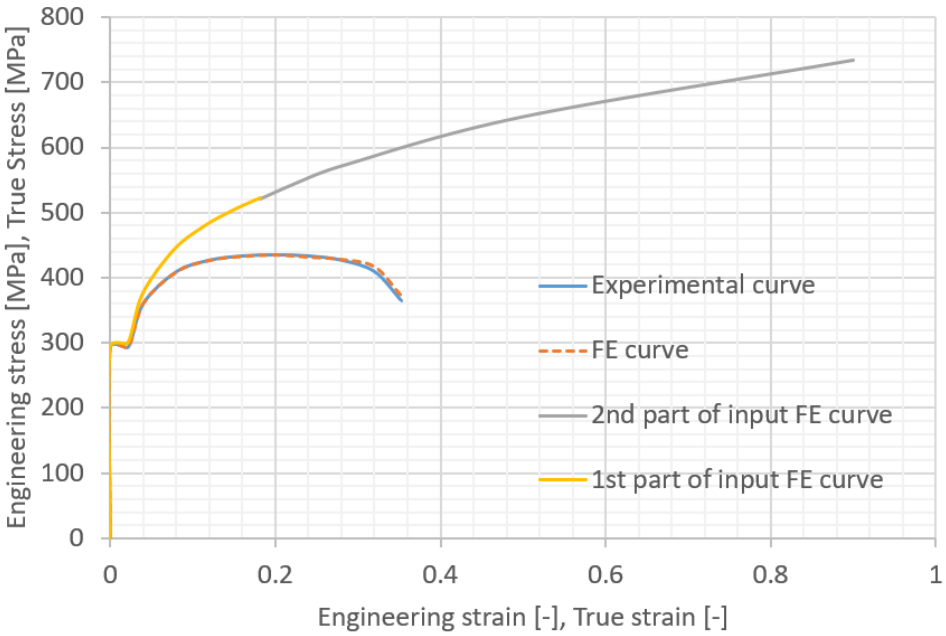

Figure 4. Stress-strain relationships for experimental (Wang et al., 2017) and numerical results.

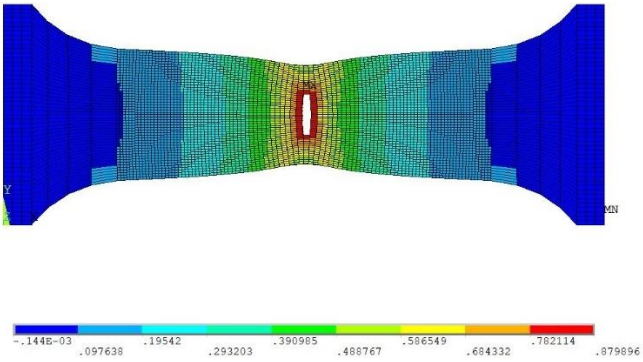

Figure 5. Strain distribution in specimen.

4. Corrosion modelling

In the present study, the two-side corrosion degradation is analysed, and the corrosion descriptors are presented in Figure 7. One can distinguish the initial thickness of the specimen as t_0 and the maximum residual thickness after corrosion degradation as t_{max}. Based on that, the uniform degree of degradation is derived as:

$$DoD_u = \frac{t_{ini} - t_{max}}{t_{ini}} \tag{6}$$

At any particular point of the corroded specimen, one can distinguish the corrosion depth in the upper surface (h_u) and in bottom surface (h_b). Similarly, there is a mean and maximum corrosion depth in both surfaces, $\overline{h_u}$ and $\overline{h_b}$ as well as Δh_u and Δh_b, respectively. The minimum residual thickness is calculated as:

$$t_{min} = t_{max} - \Delta h_u - \Delta h_b \tag{7}$$

By calculating the total volume of the corroded specimen, $V_{corroded}$, the non-uniform corrosion degradation level can be calculated as:

$$DoD_n = \frac{t_{max} \cdot A - V_{corroded}}{t_0 \cdot A} \tag{8}$$

The total degradation level is equal to:

$$DoD = DoD_u + DoD_n \tag{9}$$

The cross-sectional areas A_i (see Figure 6) are calculated along with the specimen and the minimum cross-sectional area A_{min} is obtained.

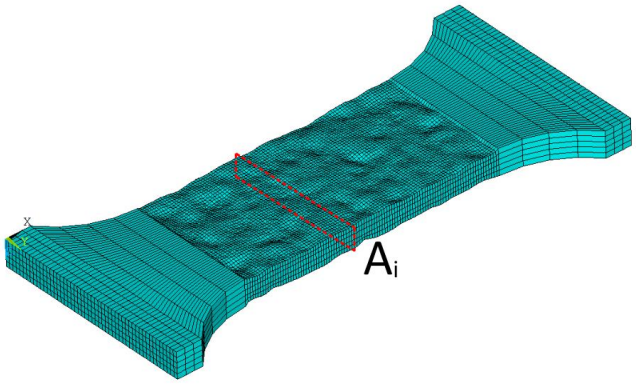

Figure 6. Corroded specimen FE model.

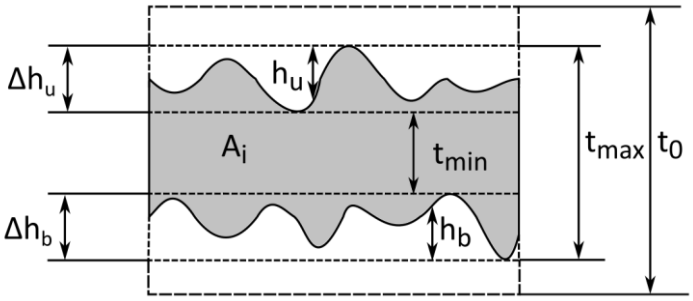

Figure 7. Corroded specimen cross-section.

To generate the random field of corroded plate surfaces, the maximum and mean corrosion depth is needed together with correlation length. For any particular mesh density, the random field is generated and then transformed into an FE model (see Figure 6). The reference thickness for the mechanical properties calculations may be different, e.g. the average thickness, maximum thickness, average thickness of the minimum cross-sectional area. (Cegla and Gajdacsi, 2016) shown that during the ultrasonic measurements of corroded plates (most common method during ship inspections), the values are usually higher than the average thickness and there are subjected to high uncertainties. Based on that, in the present study, the maximum residual thickness of corroded plates (t_{max}) was chosen as a reference one.

5. Sensitivity analysis

Different parameters related to the geometry of the specimen and random field can influence the results of the current analysis. Thus, the sensitivity analysis is conducted. The analysed parameters of the specimen and random field are presented in Table 2. The ratio between maximum corrosion depth and mean corrosion depth is assumed here equal to 3 (the value was assumed based on the observations of (Wang et al., 2017)), and thus these two variables are changed at the same time considered as one factor. The correlation length cannot be less than 0.5 mm due to the specified element size. In the case of upper value, with correlation length above 2.5 mm, the number of pits is very low, which is not observed in reality. The number of corroded surfaces is one or two, which is the one-side or two-side corroded, respectively. To keep the same minimum and maximum thickness, the corrosion degradation depth of the one-side corroded plate is two times the corrosion depth of one of the surfaces in a two-side corroded plate. Additionally, the number of realisations of the corrosion field is studied to show the difference in the results between one sample and the average value from several samples.

Table 2. Parameters of sensitivity analysis.

Variable	Initial	Minimum	Maximum
Maximum thickness [mm]	5	3	8
Maximum corrosion depth [mm]	1	0.25	1.75
Mean corrosion depth [mm]	0.333	0.083	0.583
Correlation length [mm]	1.5	0.5	2.0
Number of realisations	1	1	9
Number of corroded surfaces	2	1	2

The One factor at the Time (OFAT) methodology (Daniel, 1973) is used to perform the sensitivity analysis. Only one factor is changed, whereas the rest of the variables are equal to the initial values as

presented in Table 2. This methodology, with comparison to advanced techniques of Design of Experiments (Wu and Hamada, 2009), provides information about essential variables in a simple way, which is the main objective of the current analysis. Nevertheless, the multi-factorial analysis may be performed in further studies.

Figure 8 shows the influence of the maximum thickness into the mechanical properties. It could be noticed, that with the increase of the maximum thickness, where the other corrosion descriptors remain unchanged, the mechanical properties are growing. This phenomenon is caused by the ratio between minimal and maximum thickness. In the case of thin specimens, this ratio is much lower (for 3 mm plate it is 0.333, where for 8 mm plate it is 0.75). Due to that, any identical corrosion fields will have a more significant influence in the stress distribution in the thin specimens, compared to the thick specimens. The reduction in the yield stress ranges from 10 % in case of an 8 mm specimen up to 40 % in the case of a 3 mm thickness. In the case of the Young Modulus and ultimate stress, the reductions are between 9 % and 33 %. The most sensitive parameter is the total elongation, which is reduced between 9 % up to 78 %. The fitting curves in all cases are of the 2nd order polynomial functions, and there are shown together with the Pearson correlation factor. It can be noticed that the correlation factors are very high and thus, these curves can model the reduction of the mechanical properties in the range of thicknesses and the assumed values of the mean and maximum corrosion depths.

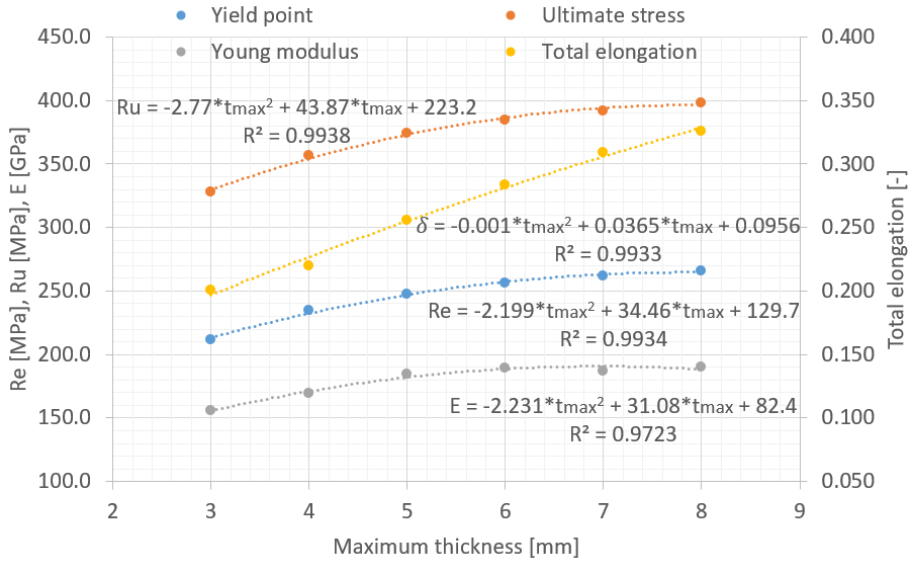

Figure 8. Mechanical properties as a function of maximum thickness.

Figure 9 shows the influence of the maximum corrosion depth, as well as the mean corrosion depth in the mechanical properties of corroded specimens. It can be noticed that when the maximum corrosion depth is growing, all mechanical properties are decreasing. This is caused by the mean thickness reduction as well as the increase of the stress concentration factors in the pit regions. The reduction of the yield stress varieties between 4% up to 29 % and ultimate stress is reduced between 3 % to 26 %. Similarly, to the initial thickness, the most sensitive variable is the total elongation, which is decreased compared to its initial value between 4 % up to 45 %. The less sensitive is the modulus of elasticity, which is reduced between 2 % up to 22 %. All parameters may be modelled with the use of the linear approximation with the high correlation factor. It could be observed that the values of these functions for $h_{max} = 0$ are the values that should be equal to the initial mechanical properties. However, small deviations are observed.

In the case of different corrosion types (one-side or two-side), the results are presented in Table 3. One can observe that there are some changes in the mechanical properties. In the case of surface 1, the results are very similar to those obtained for two-side corrosion, in the case of the Young modulus and total elongation, the values are even slightly higher. However, in the case of surface 2, the values of the yield stress and ultimate stresses are 3% and 2%, lower from two-side corrosion values, respectively. The Young modulus and total elongation are smaller of 4.5 % and 25 %, respectively. Additionally, the mean value from the two one-side corroded specimens was calculated, and the mechanical properties are lower from that obtained in the case of two-side corrosion degradation, although the same corroded surfaces were applied. Probably, the reduction is caused by higher stress concentration factors when compared with two-side corrosion.

Table 3. Results of sensitivity analysis.

Influencing factor	Value	Re [MPa]	Ru [MPa]	E [GPa]	δ [-]
Number of corroded surfaces	Upper surface corroded	246.8	374.0	190.5	0.272
	Lower surface corroded	241.4	366.5	176.9	0.204
	Mean	244.1	370.2	183.7	0.238
	Both surfaces corroded	247.8	374.0	184.8	0.256

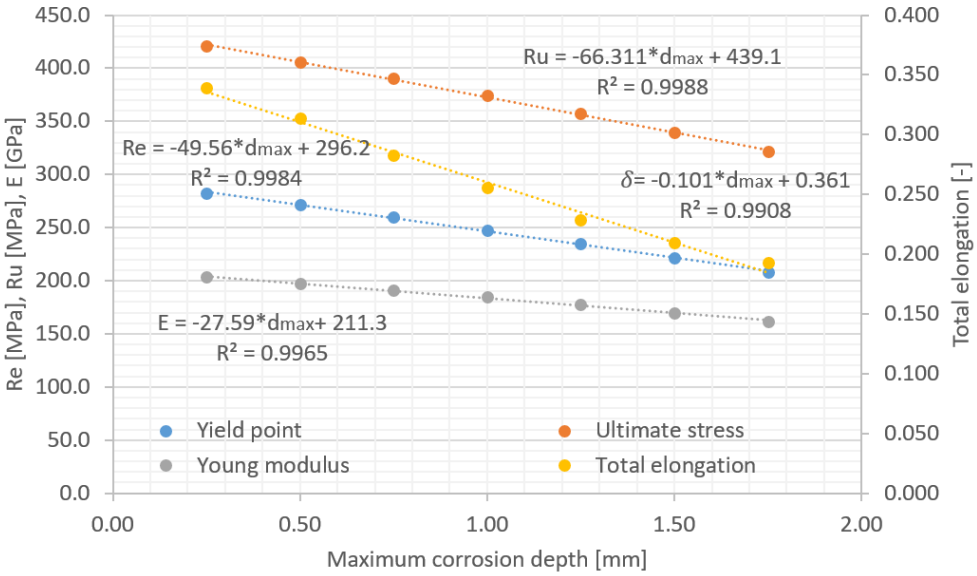

Figure 9. Mechanical properties in the function of maximum corrosion depth.

Both factors, the initial thickness and corrosion depth are investigated based on the corrosion degradation modelled with the same shape of random fields in both surfaces of corroded specimens (different between the surfaces). However, in the case of the correlation length and corrosion type, the results can deviate due to the different realisations of the specific random field. Thus, the influence of the number of random field realisations is investigated. The mechanical properties are calculated for the initial conditions with nine different realisations of the random field with the same characteristics (correlation length and mesh density). The deviations from the mean value for each realisation are presented in Figure 10.

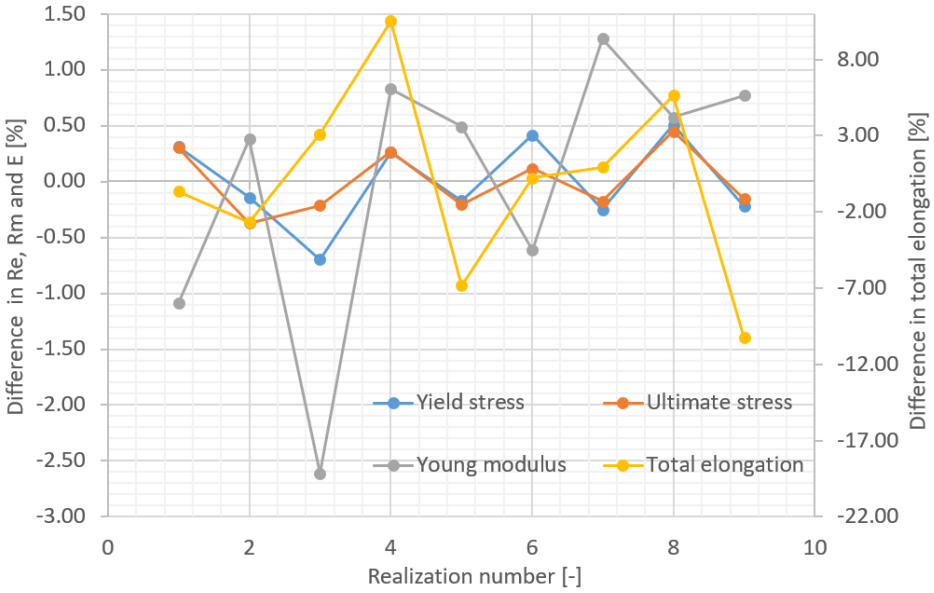

Figure 10. Deviations from the mean value for specific realisation.

The analysis shows that both yield and ultimate stresses are almost independent of the realisation number. The differences between the maximum and minimum values of these two variables are about 1 % concerning the mean value. In the case of the Young modulus, the deviations are in the order of 4 %, which is more significant. The biggest differences are in the case of the total elongation, which is reaching 20 % between the maximum and minimum value. Additionally, the correlation matrix has been developed, showing the correlation between variables. The strong correlation has been found between the yield stress and ultimate tensile stress (0.84). The moderate correlation was found between the yield stress and total elongation and between the ultimate tensile stress and total elongation with values of 0.35 and 0.58, respectively. In the case of the Young modulus, the correlation with other variables was not noted.

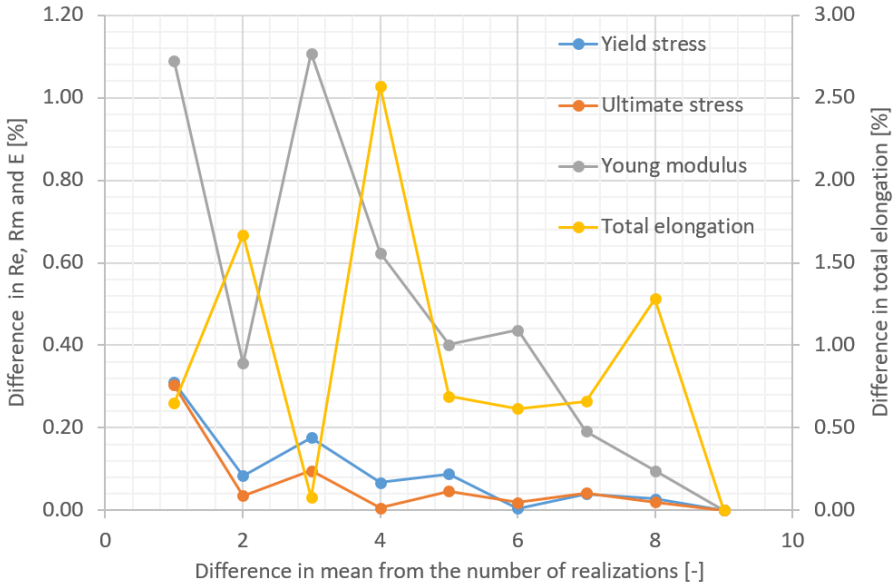

Figure 11. Convergence studies.

Due to the high level of the variation in the case of the total elongation and Young modulus, additional convergence studies based on the previous results are performed. The reason for convergence studies is to see how many samples are needed to produce a confident mean value, that is close to the mean

value from a significant amount of samples. In other words, how many samples are needed to produce the representative mean values. The results of these studies are shown in Figure 11. The differences from *n* samples are calculated as follows (x is the selected variable and $\bar{x}$ is the mean value from 9 samples):

$$D_n = \left| \frac{\sum_{i=1}^{n} \frac{x_i}{n}}{\bar{x}} - 1 \right| * 100\ \% \tag{10}$$

The analysis shows that in the case of the yield stress and ultimate stress, even one sample will be representative and two samples and more will produce minimal deviations. In the case of the Young modulus, the mean from five samples will be quite representative and will result in a difference below 0.5 % from the mean of multiple samples. Additionally, in the case of these three variables, the deviations are converging. In the case of the total elongation, no specific convergence could be distinguished. Even mean from 8 samples differ with about 1.3 % with regards to the mean from 9 samples. In this case, more samples will be needed to achieve convergence. However, concerning the difference between the minimum and maximum value, the 2% deviation level seems to be quite representative. This level of deviation may be noticed above the mean from 5 samples. Additional discussion about the sensitivity of the total elongation is discussed below.

Based on this study, one can choose the mean from a couple of samples, the most critical case or representative case to simulate the corrosion field. In further studies, the representative realisation for a specific correlation length will be chosen. The representative field is the one, that results in mechanical properties closest to mean from multiple samples. This approach will lead to less computational effort.

It could be noticed that the total elongation is subjected to high uncertainties. Probably, the total elongation is dependent on specific corrosion field, which could be seen in different failure schemes (Figure 12) for specimens with the same field descriptors. The failure modes for nine realisations are presented. Generally, the reduction of the total elongation is related to premature breaking due to the stress concentration in the region of the pit, which may be visible in the strain distribution of the corroded specimen. It can also be noticed that the breaking line is not perpendicular to the longitudinal direction of the specimen. Breaking may also not be located in the middle-length of the specimen, and it seems to be dependent on the location of the minimum cross-sectional area.

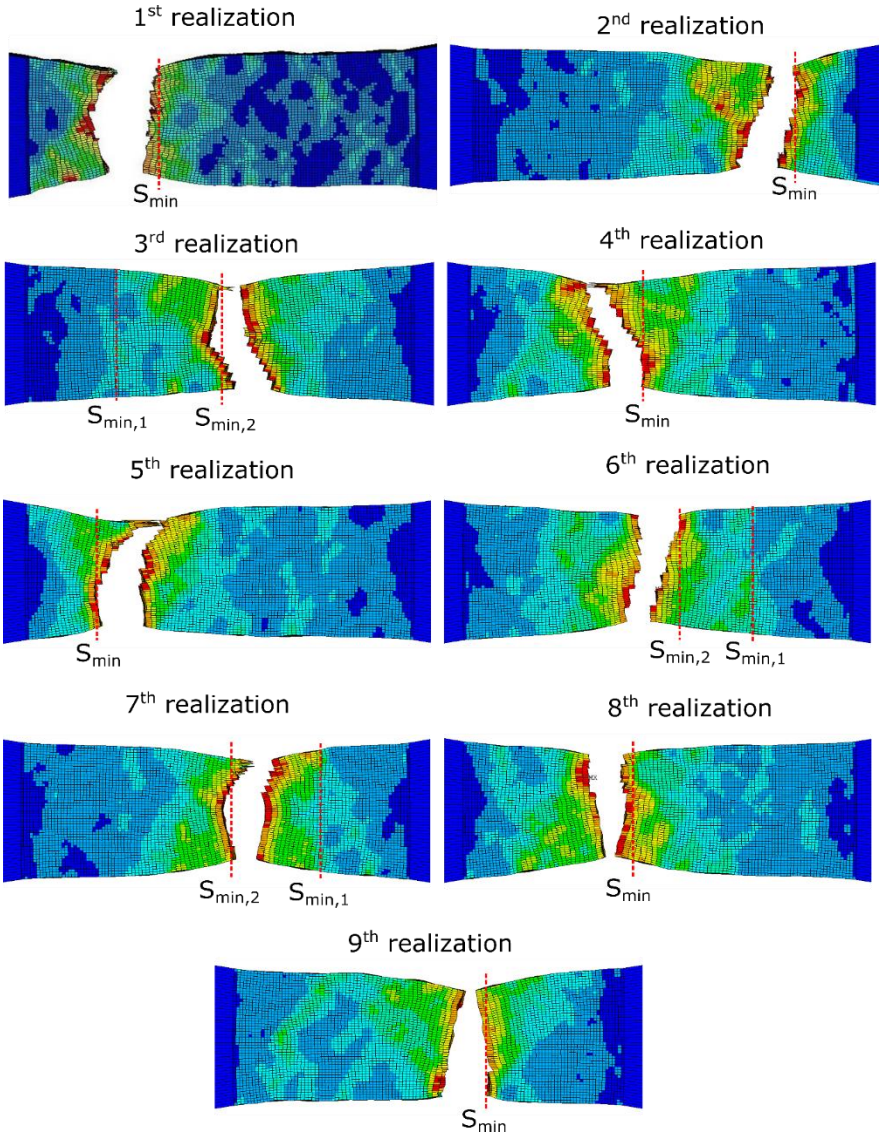

Figure 12. Failure schemes of specimens with different realisations of the random field.

The hypothesis that the breaking line is correlated with the minimum cross-sectional area is verified. The positions of the minimum cross-sections, together with actual breaking positions, are presented in Figure 15. If the first position of the minimum cross-sectional area is not coherent with the breaking position, the second smallest one is found.

It can be noticed that the positions of the minimum cross-sectional area are the same as the position of the breaking region. Thus, it can be concluded that the breaking will occur in the region of the minimum cross-sectional area of one of two minimum cross-sectional areas (in the case of three realisations). In the case of specimens, where the second smallest cross-sectional area broke, the stress concentration about pit regions could be the reason for that.

Figure 13 shows the impact of the correlation length of the random field into the mechanical properties. For each correlation length, the representative fields for upper and lower corroded surfaces were chosen, as described previously. The correlation length has almost no influence in both yield stress and ultimate stress (the differences between maximum and minimum value are in the order of 2%). The minimal impact can be visible in the case of the Young modulus (difference of 7% between maximum and minimum value). However, it is hard to find any correlation with correlation length, which is represented by a small Pearson factor. It could be concluded that the deviations are

stochastically originated. The only significant effect that can be noticed is concerning the total elongation. In this case, with the increase of the correlation length, the total elongation is reduced. Similarly, to other factors, the total elongation is the most sensitive variable.

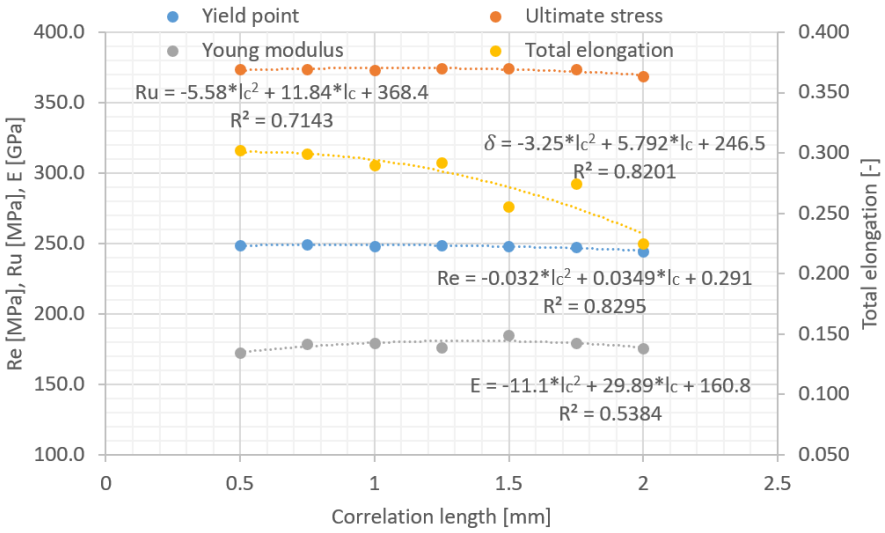

Figure 13. Mechanical properties as a function of the correlation length.

Based on the sensitivity analysis, one can conclude, that the maximum thickness and mean corrosion depth are the most sensitive parameters that govern the reduction of mechanical properties. Almost no influence is visible in the case of the correlation length and type of corrosion (one-side or two-side). The only variable that shows some sensitivity concerning the correlation length is the total elongation. However, the studies revealed that the total elongation is the most sensitive concerning all parameters, and it is subjected to high uncertainties, which was shown in the random field convergence studies. The Young modulus is also subjected to some uncertainty. Most certain parameters are the yield stress together with ultimate tensile stress. In order to see the influence of different factors, acting simultaneously, the multi-factorial analysis needs to be conducted.

6. Finite element analysis of corroded specimens

For evaluation of newly developed methodology, a numerical analysis of the corroded specimens is performed and validated with the experimental analysis as presented in (Wang et al., 2017). The specimens were taken from the steel truss (made from H-beam elements), which was exposed to natural environmental conditions. The nine specimens were taken and analysed from horizontal (H), sloping (S) and vertical (V) members. One specimen was cut from the top flange (TF), one from the bottom flange (BF) and one from the web (W) for each type of member. The basic parameters of the random fields are equivalent to those measured experimentally, i.e. maximum and mean corrosion depths of both surfaces. The dimensions of the specimens and maximum thicknesses of the specimens are satisfied as well. The material properties are calibrated to obtain the experimental stress-strain curve in the intact conditions, as presented in Section 3. The main dimensions and descriptors of the corrosion fields are presented in Table 6. All parameters are precisely identical in numerical simulations.

Table 6. Specimens descriptions.

Specimen	t_0 [mm]	t_{max} [mm]	$h_{u,max}$ [mm]	$\overline{h_u}$ [mm]	$h_{b,max}$ [mm]	$\overline{h_b}$ [mm]	t_{min} [mm]
HTF	9	7.98	0.331	0.113	1.253	0.515	6.4
HBF	9	7.93	0.945	0.361	1.106	0.399	5.88

HW	6.5	5.28	0.868	0.286	0.692	0.298	3.72
STF	9	7.86	0.437	0.134	1.282	0.466	6.14
SBF	9	7.8	0.737	0.228	0.91	0.341	6.15
SW	6.5	5.27	0.888	0.247	1.097	0.385	3.29
VTF	8	7.36	0.466	0.152	0.751	0.192	6.14
VBF	8	7.3	0.81	0.279	0.73	0.171	5.76
VW	6	5.42	0.593	0.163	0.487	0.179	4.24

The only parameter that is related to correlation length is the number of corrosion pits per square centimetre. Since the correlation length has not such a significant influence in mechanical properties, two different correlation lengths are chosen to simulate the corroded surfaces and made the analysis more simple. The correlation length equals to 1 mm was chosen to model the surfaces with a denser pitting distribution (above 10), whereas correlation length of 1.5 mm was chosen to model the surfaces with a lower number of pits per square centimetre (below 10). The comparison of the experimentally measured and simulated surfaces is presented in Figure 14, and one can see that there are quite similar between each other. The comparison between surfaces in the experiment and numerical predictions is presented in Table 7.

Based on the sensitivity analysis, one can notice that at least a couple of samples will need to produce proper results. However, to avoid multiple calculations, two representative fields for each correlation length were chosen to produce results close to the mean from a couple of samples. One can notice small deviations in the minimum cross-sectional area between numerical and experimental predictions. There are originated from the differences between the real corrosion fields and randomly generated ones. When maximum corrosion depth together with the mean corrosion depth is satisfied, the minimum cross-sectional area is the resulting value.

Table 7. Experimental and numerical corrosion field descriptors.

Specimen	DoD_u [%]	DoD_n [%]	DoD [%]	A_{min} $[mm^2]$	A_{min} numerical $[mm^2]$	$\frac{Pits}{cm^2}$ Upper surface	$\frac{Pits}{cm^2}$ Bottom surface	$c_{0,u}$ [mm]	$c_{0,b}$ [mm]
HTF	11.3	9.5	20.8	180.4	179.3	20.2	6.4	1	1.5
HBF	11.9	11.9	23.8	173.7	173.0	6.9	7.5	1.5	1.5
HW	18.8	10.5	29.3	115.3	112.6	9.4	11.5	1.5	1
STF	12.7	10.5	23.2	177.7	176.7	15.7	7.6	1	1.5
SBF	13.3	8.9	22.2	177.2	176.5	13.4	10.7	1	1
SW	18.9	14.7	33.6	112.1	110.2	8.6	6.8	1.5	1.5
VTF	8.0	8.9	16.9	173.4	172.4	15.3	14.6	1	1
VBF	8.7	10.5	19.2	168.5	167.5	11	13.3	1	1
VW	9.7	9.8	19.5	124.3	124.2	12.2	14.5	1	1

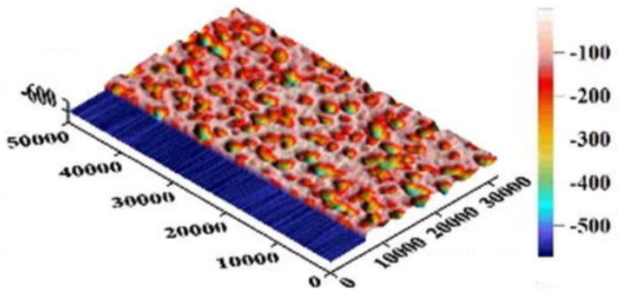

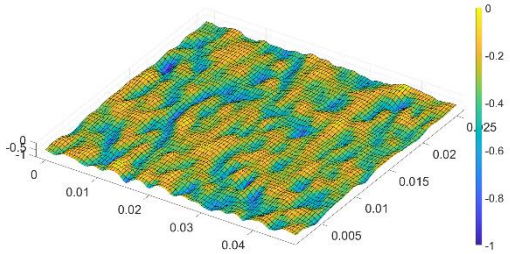

Figure 14. Real corrosion field of VW upper surface (Wang et al., 2017) (left) with randomly generated corrosion field (right).

The results of the numerical analysis using the random field approach compared to experimental tests are presented in Table 8. The lowest deviations between experimental and numerical results are in the case of the ultimate stress, where the mean error is 1 %. In the case of the Young modulus and yield stress, the mean error is about 2 %. The most significant mean error is for the total elongation, which is equal to 7%. However, only for severely corroded specimens (HW and SW), the error is 20 %. For the rest of the specimens, the error of total elongation does not exceed 6 %.

Table 8. Results of analysis.

Specimen	R_e [MPa] (Wang et al., 2017)	R_e [MPa] num.	R_u [MPa] (Wang et al., 2017)	R_u [MPa] num.	E [GPa] (Wang et al., 2017)	E [GPa] num.	δ [%](Wang et al., 2017)	δ [%] num.
HTF	268.2	266.7	402.7	399.0	194.6	190.9	31.7	31.3
HBF	263.8	261.8	399.7	392.4	184.5	187.4	31.3	32.0
HW	250.7	256.8	384.5	385.6	189.7	188.7	24.1	28.9
STF	267.0	267.2	403.6	400.0	200.3	191.3	31.5	31.3
SBF	268.1	268.2	407.1	402.1	198.9	192.4	32.4	34.0
SW	242.4	252.0	388.2	380.3	187.3	179.7	21.6	26.0
VTF	264.8	277.7	415.6	413.6	203.9	198.1	32.3	34.3
VBF	264.5	272.9	412.0	407.1	200.7	194.5	31.8	33.7
VW	271.6	272.3	412.5	405.9	195.4	195.5	30.8	32.4
Error [%]	0.0 - 4.9		0.2 - 1.8		0.1 – 4.5		0.6 – 20.2	

One can notice that except the total elongation, which is a very sensitive parameter, the deviations are not significant. They are much smaller concerning the deviations between experimental tests and results from different mathematical models that were presented in (Wang et al., 2017), which were in the order of 16 % in case of the yield strength. Nevertheless, the deviations are in the same order with deviations between experimental and numerical results obtained in (Wang et al., 2017), where the FE analysis was performed, and the corrosion fields were identical with those measured experimentally. Additionally, the results of the proposed methodology are the results of a single random field realisation, which is close to the mean value from a couple of samples. However, the sample that produces maximum or minimum mechanical properties can be possibly more representative and closer to the real specimen. In the case of an experiment, it is hard to produce two samples with the same corrosion field descriptors (maximum corrosion depth and mean corrosion depth).

The deviations between the numerical and experimental results may originate not only from the corrosion modelling differences but also from the material properties deviations in the experimental domain as well as uncertainty measurement. The results of tensile tests for intact specimens (Li and Pasternak, 2019) show, that coefficient of variation in the case of the yield strength is 5 % and in the case of the ultimate stress is 1.5 %. In this point of view, the deviations between the numerical and experimental results are similar to these values. Due to that, the results are additionally compared with the numerical simulations of (Wang et al., 2017), where the same specimens with corrosion surfaces transmitted to the FE model were analysed. In this case, the input material properties are always the same. The results of the comparison are presented in Table 9.

Table 9. Results of analysis.

Specimen	R_e [MPa] (Wang et al., 2017) num.	R_e [MPa] num.	R_u [MPa] (Wang et al., 2017) num.	R_u [MPa] num.	E [GPa] (Wang et al., 2017) num.	E [GPa] num.	δ [%](Wang et al., 2017) num.	δ [%] num.
HTF	267.2	266.7	402.0	399.0	195.6	190.9	33.4	31.3
HBF	264.3	261.8	398.0	392.4	193.8	187.4	33.5	32.0
HW	249.2	256.8	388.6	385.6	185.7	188.7	26.8	28.9
STF	268.2	267.2	402.5	400.0	196.6	191.3	33.7	31.3
SBF	268.7	268.2	404.6	402.1	197.5	192.4	32.2	34.0
SW	248.2	252.0	390.1	380.3	183.1	179.7	24.6	26.0
VTF	275.0	277.7	411.4	413.6	200.0	198.1	33.6	34.3
VBF	271.2	272.9	408.8	407.1	199.2	194.5	34.0	33.7
VW	275.3	272.3	409.6	405.9	201.4	195.5	33.3	32.4
Error [%]	0.2 - 3.0		0.4 - 2.5		1.0 – 3.3		0.9 – 7.8	

It can be noticed that the error is smaller concerning the comparison between the experimental predictions and random approach. Especially in the case of the total elongation, the maximum deviation is significantly reduced. The deviations shown in Table 8 are in the same order as the deviations between the exact FE model and experiment. Additionally, the deviations between the random field modelling and accurate FE modelling are in the order of the differences resulting from a couple of generations of the specific random field. One can notice, that single analysed specimen can be represented by the randomly modelled one with either the maximum mechanical properties or minimum between a couple of simulations. From that point of view, stochastic modelling provides accurate results concerning the mechanical properties of the corroded specimens. Additionally, some specific FE modelling differences may impact the differences in the results. The comparison between experimental and numerical results as presented in (Wang et al., 2017) with comparison to the presented methodology is shown in Figures 15 – 18.

The yield stress presented as a function of DoD is shown in Figure 15. One can notice that both curves, showing numerical predictions, are very close to each other, and there are modelled with the use of a linear approximation with highly correlated factors. In the case of the experimental curve, the best fitting curve is the polynomial one, and it deviates from the numerical predictions in the low values of DoD. However, the curves should tend to the initial value of the yield stress for DoD equals to 0, which could be observed for numerical curves. Thus, the possible deviations of the experimental curve may originate from the variability of the initial mechanical properties. Mainly, it could be noticed that two points for DoD close to 19 % differ significantly in the experimental results. In the case of numerical predictions, the two points are close to each other.

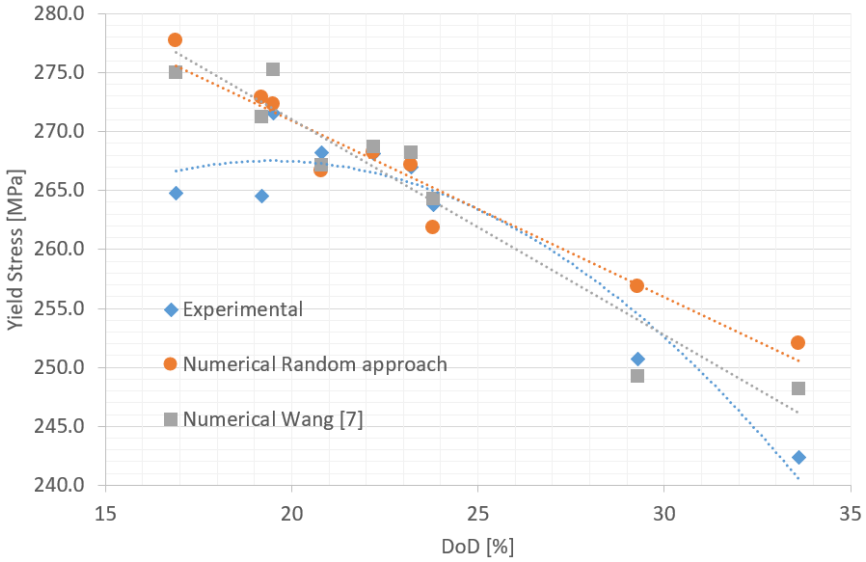

Figure 15. Yield stress in the function of DoD.

Figure 16 shows the ultimate stress as a function of DoD. In this case, all regression curves are linear with high correlation factors. It may be observed that all curves are very close to each other. However, the experimental curve shows slightly higher values compared to other ones. All curves tend to the value, which is very close to the initial ultimate stress when DoD equals to 0.

The Young modulus presented as a function of DoD is presented in Figure 17. Similarly, to the ultimate stress, the best regression curves are linear. In the case of the numerical predictions, the coefficients of determination are high, whereas the coefficient of determination in the case of the experimental curve is quite low (0.52). The possible reason for that is the measuring uncertainty, which is related to the extensometer usage in the testing procedure. The deviations between the two numerical approaches may result from different parallel lengths, which were taken to measure the elongation in the first part of the stress-strain curve. Additionally, the curves are crossing the vertical axis for DoD equals to 0 with values close to the initial Young modulus.

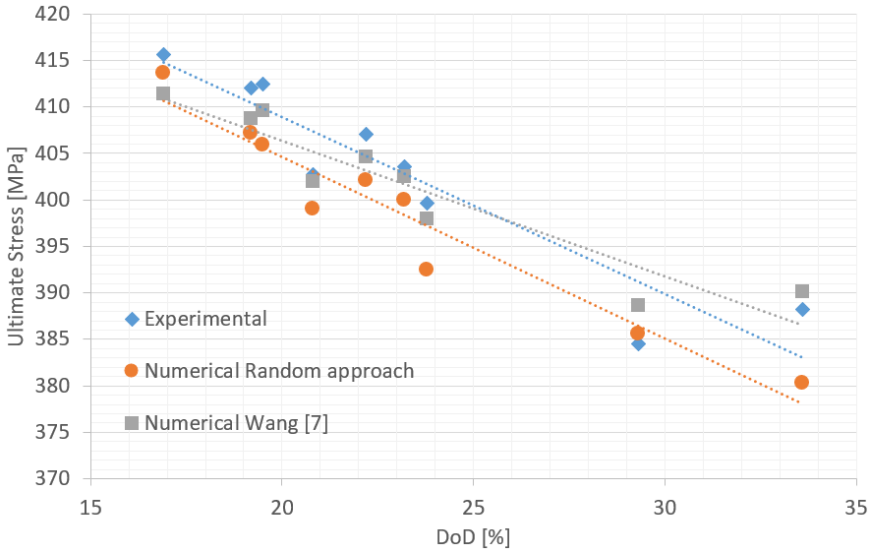

Figure 16. Ultimate stress as a function of DoD.

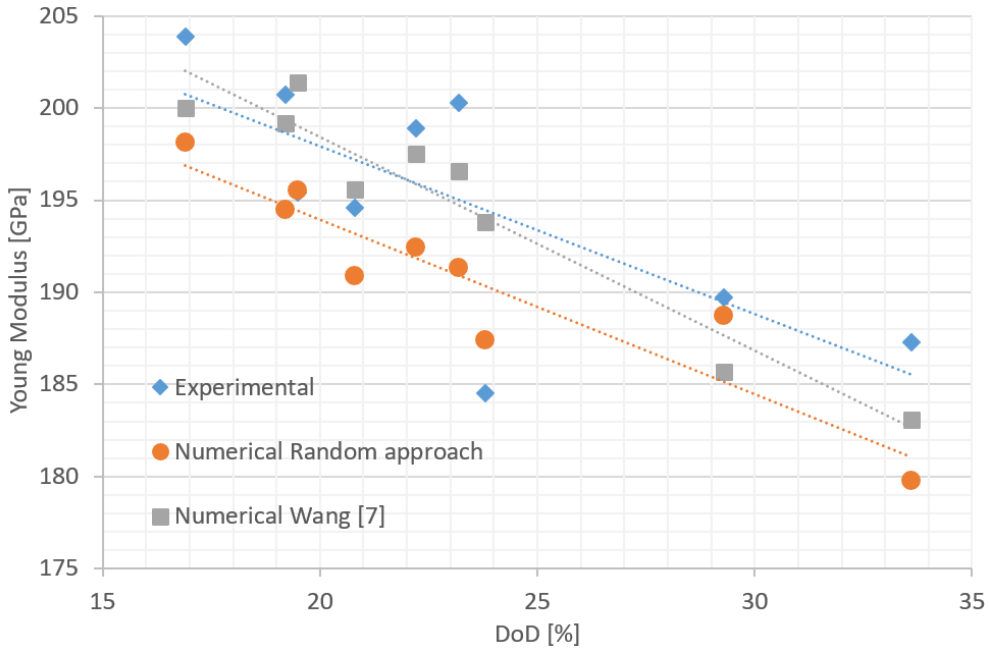

Figure 17. Young modulus as a function of DoD.

Figure 18 shows the total elongation in the function of DoD. In this case, the polynomial fitting curves are used to model the change of the total elongation concerning the DoD. In all cases, the correlation factors are very high. Similarly, to other mechanical properties, all three curves are quite similar. However, the methodology, which is used in this study, slightly overestimates the total elongation in the higher values of DoD. It may be explained with the representative random field that was chosen to model the corrosion fields. When the most critical random field is chosen, the values could be much closer to those obtained experimentally. For DoD equals to 0, the numerical predictions using a random approach shows a value close to the initial total elongation. In other cases, these values are quite outstanding.

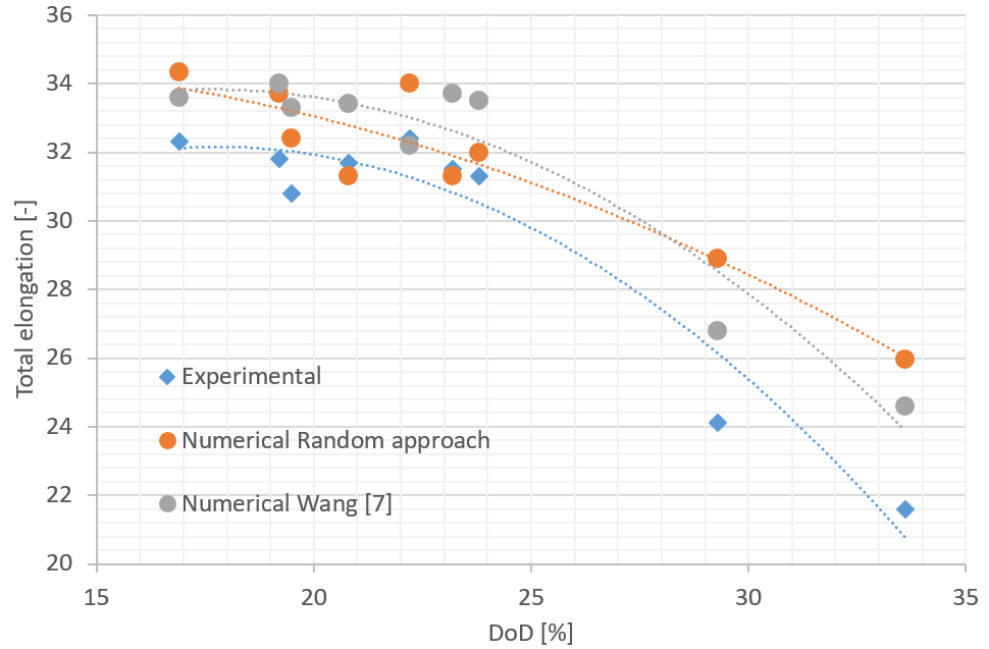

Figure 18. Total elongation as a function of DoD.

Based on the presented results, one can notice that the FE analysis of the corroded specimens with randomly generated corrosion fields is very close to the experiment. Additionally, the FE analysis with randomly generated corrosion degradation is almost identical to the FE analysis with real corrosion fields.

The comparison between the experimental stress-strain curves and numerically obtained ones with the use of the current methodology is presented in Figure 19. As it can be noticed, for all specimens, the curves are very similar to each other. This leads to the conclusion that not only mechanical properties are similar, but the general stress-strain response match as well.

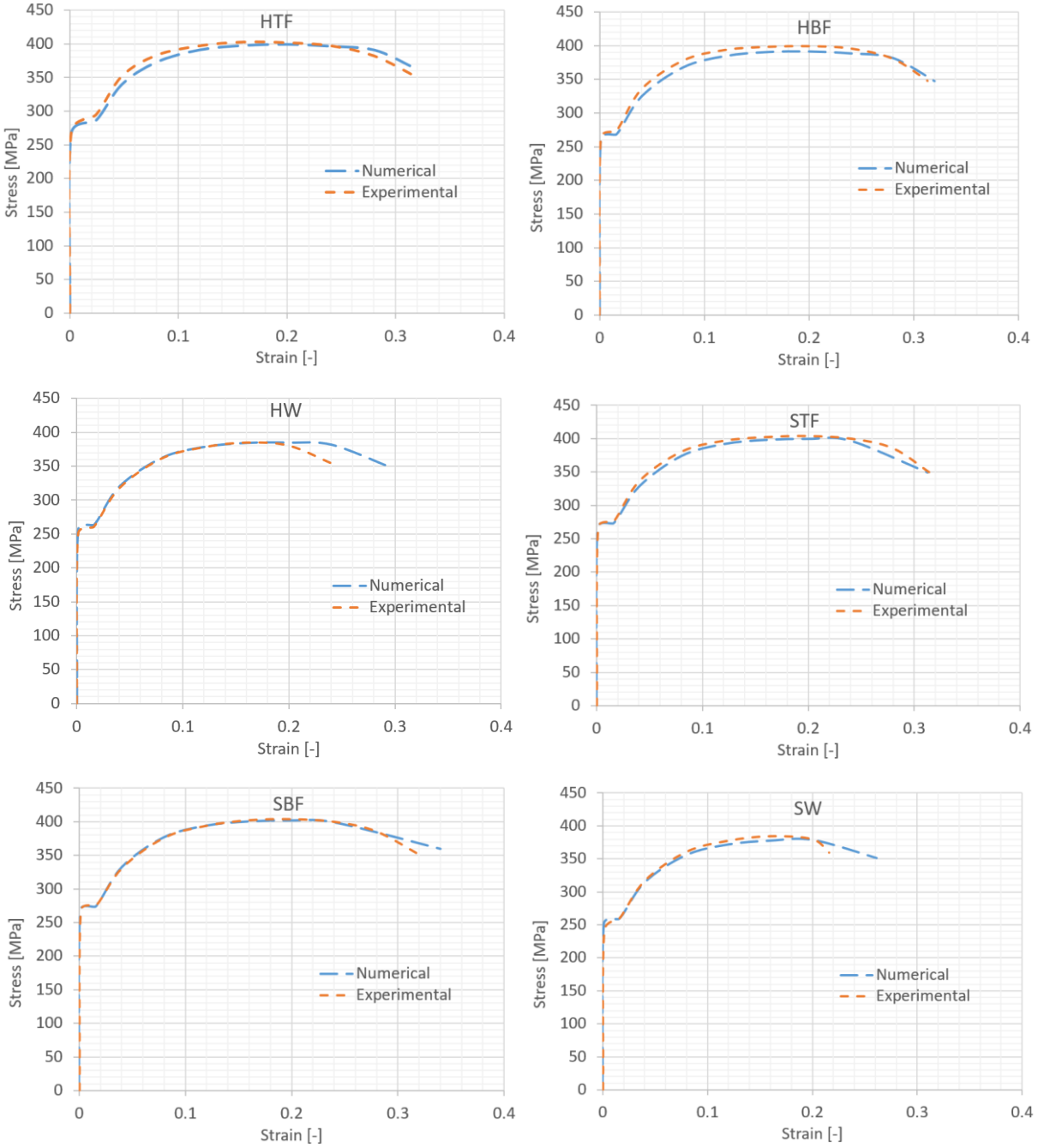

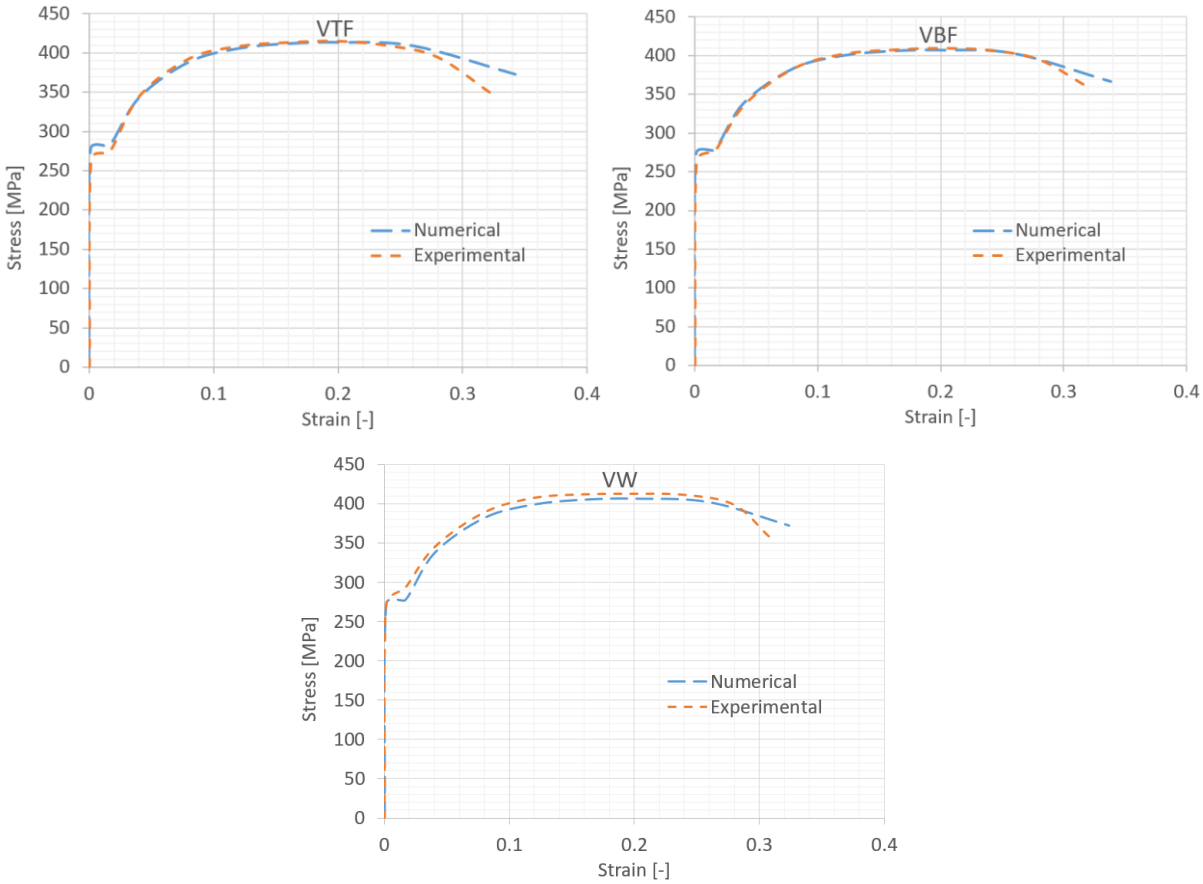

Figure 19. Stress-strain curves for all specimens.

7. Conclusions

The methodology presented in this work revealed to be practical for the evaluation of the mechanical properties of corroded steel specimens. The random field modelling may provide the morphology of the corroded surface very similar to the real one. Compared to very thin plates, even for higher values of Degree of Degradation, the results are comparable to the experimental ones. This leads to the conclusion that the irregularities in the corroded surfaces are the factor that predominantly governs the mechanical properties reduction.

The random field modelling has another advantage. Using random field techniques, one can generate many samples, which is challenging in other cases due to the long duration of the corrosion process as well as a very functional analysis of the corrosion morphology and in this way, it is economically justified. Nevertheless, more experimental work should be done to validate furtherly of the proposed methodology. Possibly the changes in the mechanical properties may vary depending on corrosion type and other factors (marine, atmospheric, etc.).

The corrosion degradation with the same average and maximum depth value will cause a much higher reduction of the mechanical properties in the thinner plates compared to thicker plates. Additionally, the reduction seems to be higher in the thinner plates for similar DoD compared to the thicker plates. The following conclusions may be derived when the presented results are compared with the investigations related to very thin specimens (Woloszyk and Garbatov, 2020).

Based on the sensitivity analysis, it can be observed that the mechanical properties changes due to corrosion process are susceptible concerning the initial thickness of plates as well as the maximum and mean corrosion depth values. Some sensitivity concerning the type of corrosion (one-side or two-side)

is visible as well. In this case, the one-side corrosion will be the worst case. The correlation length of the corrosion field revealed to be not a very sensitive parameter within the considered range. However, the total elongation was slightly reduced for the higher values of the correlation length. The total elongation revealed to be subjected to a high level of uncertainties, and it is the most sensitive parameter concerning the input parameters. Thus, the higher deviations between the numerical predictions and experimental results in terms of this variable may be justified. Finally, one needs to be aware, that presented foundings are related to small-scale specimens subjected to tensile loading and yielding failure. The mechanical behaviour of corroded specimens with different scales and subjected to different types of loads need to be furtherly investigated.

The deviations between the numerical and experimental results may originate from the uncertainties in the initial mechanical properties. This is additionally supported by the comparison of the numerical predictions with the use of the random approach and exact FE model of corroded specimens. In this case, where the input mechanical properties were identical, the deviations between both models were minimal.

Acknowledgements

This work has been supported by the National Science Centre, Poland (grant No. 2018/31/N/ST8/02380). The ANSYS software used in presented simulations in this paper was available as a part of the partnership cooperation agreement between ANSYS Inc., MESco sp. z o.o. and the Gdansk University of Technology. Part of the calculations was carried out at the Academic Computer Centre in Gdańsk.

References

Ahmmad, M.M., Sumi, Y., 2010. Strength and deformability of corroded steel plates under quasi-static tensile load. J. Mar. Sci. Technol. 15, 1–15. https://doi.org/10.1007/s00773-009-0066-1

ANSYS Inc., 2019. ANSYS LS-DYNA User's Guide.

Appuhamy, J.M.R.S., Kaita, T., Ohga, M., Fujii, K., 2011. Prediction of residual strength of corroded tensile steel plates. Int. J. Steel Struct. 11, 65–79. https://doi.org/10.1007/S13296-011-1006-6

Bäker, M., 2018. How to get meaningful and correct results from your finite element model.

Cairns, J., Plizzari, G.A., Du, Y., Law, D.W., Franzoni, C., 2005. Mechanical properties of corrosion-damaged reinforcement. ACI Mater. J. 102, 256–264.

Cegla, F., Gajdacsi, A., 2016. Mitigating the effects of surface morphology changes during ultrasonic wall thickness monitoring, in: AIP Conference Proceedings. p. 170001. https://doi.org/10.1063/1.4940624

Constantine, P., 2012. Random Field Simulation [WWW Document]. URL https://www.mathworks.com/matlabcentral/fileexchange/27613-random-field-simulation (accessed 11.26.19).

Daniel, C., 1973. One-at-a-Time Plans. J. Am. Stat. Assoc. 68, 353–360. https://doi.org/10.1080/01621459.1973.10482433

Du, Y.G., Clark, L.A., Chan, A.H.C., 2005a. Residual capacity of corroded reinforcing bars. Mag. Concr. Res. 57, 135–147. https://doi.org/10.1680/macr.57.3.135.60482

Du, Y.G., Clark, L.A., Chan, A.H.C., 2005b. Effect of corrosion on ductility of reinforcing bars. Mag. Concr. Res. 57, 407–419. https://doi.org/10.1680/macr.2005.57.7.407

Fernandez, I., Bairán, J.M., Marí, A.R., 2016. Mechanical model to evaluate steel reinforcement corrosion effects on σ-ε and fatigue curves. Experimental calibration and validation. Eng. Struct. 118, 320–333. https://doi.org/10.1016/j.engstruct.2016.03.055

Fernandez, I., Berrocal, C.G., 2019. Mechanical Properties of 30 Year-Old Naturally Corroded Steel Reinforcing Bars. Int. J. Concr. Struct. Mater. 13, 9. https://doi.org/10.1186/s40069-018-0308-x

Flaks, V.Y., 1978. Correlation of pitting corrosion of aluminum plates and reduction of load-bearing capacity under tension. Sov. Mater. Sci. 14, 75–78. https://doi.org/10.1007/BF00731976

Garbatov, Y., Guedes Soares, C., 2017. Spatial Corrosion Wastage Modelling of Steel Plates Subjected to Marine Environments, in: Volume 9: Offshore Geotechnics; Torgeir Moan Honoring Symposium. American Society of Mechanical Engineers. https://doi.org/10.1115/OMAE2017-61751

Garbatov, Y., Guedes Soares, C., Parunov, J., 2014a. Fatigue strength experiments of corroded small scale steel specimens. Int. J. Fatigue 59, 137–144. https://doi.org/10.1016/j.ijfatigue.2013.09.005

Garbatov, Y., Guedes Soares, C., Parunov, J., Kodvanj, J., 2014b. Tensile strength assessment of corroded small scale specimens. Corros. Sci. 85, 296–303. https://doi.org/10.1016/j.corsci.2014.04.031

Garbatov, Y., Guedes Soares, C., Wang, G., 2006. Nonlinear Time Dependent Corrosion Wastage of Deck Plates of Ballast and Cargo Tanks of Tankers. J. Offshore Mech. Arct. Eng. 129, 48–55. https://doi.org/10.1115/1.2426987

Garbatov, Y., Saad-Eldeen, S., Guedes Soares, C., Parunov, J., Kodvanj, J., 2018. Tensile test analysis of corroded cleaned aged steel specimens. Corros. Eng. Sci. Technol. 1–9. https://doi.org/10.1080/1478422X.2018.1548098

Ghanem, R.G., Spanos, P.D., 1991. Stochastic Finite Elements: A Spectral Approach, Stochastic Finite Elements: A Spectral Approach. Springer New York, New York, NY. https://doi.org/10.1007/978-1-4612-3094-6

Górski, J., Mikulski, T., Oziębło, M., Winkelmann, K., 2015. Effect of geometric imperfections on aluminium silo capacities. Stahlbau 84, 52–57. https://doi.org/10.1002/stab.201510224

Górski, J., Winkelmann, K., 2017. Generation of random fields to reflect material and geometric imperfections of plates and shells, in: Shell Structures: Theory and Applications Volume 4. CRC Press, pp. 537–540. https://doi.org/10.1201/9781315166605-124

ISO, 2009. Metallic materials - Tensile testing - Part 1: Method of test at room temperature. Int. Stand. ISO 6892-1.

Jankowski, R., Walukiewicz, H., 1997. Modeling of two-dimensional random fields. Probabilistic Eng. Mech. 12, 115–121. https://doi.org/10.1016/S0266-8920(96)00040-9

Kashani, M.M., Crewe, A.J., Alexander, N.A., 2013. Nonlinear stress-strain behaviour of corrosion-damaged reinforcing bars including inelastic buckling. Eng. Struct. 48, 417–429. https://doi.org/10.1016/j.engstruct.2012.09.034

Kwesi Nutor, R., 2017. Using the Hollomon Model to Predict Strain-Hardening in Metals. Am. J. Mater. Synth. Process. 2, 1–4. https://doi.org/10.11648/j.ajmsp.20170201.11

Li, C., Der Kiureghian, A., 1993. Optimal Discretization of Random Fields. J. Eng. Mech. 119, 1136–1154. https://doi.org/10.1061/(ASCE)0733-9399(1993)119:6(1136)

Li, D., Xiong, C., Huang, T., Wei, R., Han, N., Xing, F., 2018. A simplified constitutive model for corroded steel bars. Constr. Build. Mater. 186, 11–19. https://doi.org/10.1016/j.conbuildmat.2018.07.019

Li, L., Li, C.-Q., Mahmoodian, M., 2019. Effect of Applied Stress on Corrosion and Mechanical Properties of Mild Steel. J. Mater. Civ. Eng. 31, 04018375. https://doi.org/10.1061/(ASCE)MT.1943-5533.0002594

Li, L., Mahmoodian, M., Li, C.Q., 2018. Effect of corrosion on mechanical properties of steel bridge elements, in: 9th INTERNATIONAL CONFERENCE ON BRIDGE MAINTENANCE, SAFETY AND MANAGEMENT.

Li, Z., Pasternak, H., 2019. Experimental and numerical investigations of statistical size effect in S235JR steel structural elements. Constr. Build. Mater. 206, 665–673. https://doi.org/10.1016/j.conbuildmat.2019.02.106

Mathworks, 2019. Matlab R2019b.

Melchers, R., 2017. Structural Reliability Analysis and Prediction. John Wiley & Sons Ltd, Chichester, UK. https://doi.org/10.1002/9781119266105

Melchers, R.E., 2008. Development of new applied models for steel corrosion in marine applications including shipping. Ships Offshore Struct. 3, 135–144. https://doi.org/10.1080/17445300701799851

Moreno, E., Cobo, A., Palomo, G., González, M.N., 2014. Mathematical models to predict the mechanical behavior of reinforcements depending on their degree of corrosion and the diameter of the rebars. Constr. Build. Mater. 61, 156–163. https://doi.org/10.1016/j.conbuildmat.2014.03.003

Nakai, T., Matsushita, H., Yamamoto, N., Arai, H., 2004. Effect of pitting corrosion on local strength of hold frames of bulk carriers (1st report). Mar. Struct. 17, 403–432. https://doi.org/10.1016/j.marstruc.2004.10.001

Nie, B., Xu, S., Yu, J., Zhang, H., 2019. Experimental investigation of mechanical properties of corroded cold-formed steels. J. Constr. Steel Res. 162, 105706. https://doi.org/10.1016/j.jcsr.2019.105706

Paik, J.K., Thayamballi, A.K., Park, Y. Il, Hwang, J.S., 2004. A time-dependent corrosion wastage model for seawater ballast tank structures of ships. Corros. Sci. 46, 471–486. https://doi.org/10.1016/S0010-938X(03)00145-8

Palsson, R., Mirza, M.S., 2002. Mechanical response of corroded steel reinforcement of abandoned concrete bridge. ACI Struct. J. 99, 157–162.

Qin, G., Xu, S., Yao, D., Zhang, Z., 2016. Study on the degradation of mechanical properties of corroded steel plates based on surface topography. J. Constr. Steel Res. 125, 205–217. https://doi.org/10.1016/j.jcsr.2016.06.018

Saad-Eldeen, S., Garbatov, Y., Guedes Soares, C., 2012. Effect of corrosion degradation on ultimate strength of steel box girders. Corros. Eng. Sci. Technol. 47, 272–283. https://doi.org/10.1179/1743278212Y.0000000005

Teixeira, Â.P., Guedes Soares, C., 2008. Ultimate strength of plates with random fields of corrosion. Struct. Infrastruct. Eng. 4, 363–370. https://doi.org/10.1080/15732470701270066

Teixeira, A.P., Ivanov, L.D., Guedes Soares, C., 2013. Assessment of characteristic values of the ultimate strength of corroded steel plates with initial imperfections. Eng. Struct. 56, 517–527.

https://doi.org/10.1016/j.engstruct.2013.05.002

Wang, Y., Wharton, J.A., Shenoi, R.A., 2014. Ultimate strength analysis of aged steel-plated structures exposed to marine corrosion damage: A review. Corros. Sci. 86, 42–60. https://doi.org/10.1016/j.corsci.2014.04.043

Wang, Y., Xu, S., Wang, H., Li, A., 2017. Predicting the residual strength and deformability of corroded steel plate based on the corrosion morphology. Constr. Build. Mater. 152, 777–793. https://doi.org/10.1016/j.conbuildmat.2017.07.035

Woloszyk, K., Garbatov, Y., 2020. Random field modelling of mechanical behaviour of corroded thin steel plate specimens. Eng. Struct. 212, 110544. https://doi.org/10.1016/j.engstruct.2020.110544

Woloszyk, K., Garbatov, Y., 2019a. Uncertainty assessment of ultimate strength of corroded stiffened plates subjected to maintenance, in: Georgiev, P., Soares, C.G. (Eds.), Sustainable Development and Innovations in Marine Technologies. CRC Press, pp. 429–436. https://doi.org/10.1201/9780367810085-57

Woloszyk, K., Garbatov, Y., 2019b. Structural Reliability Assessment of Corroded Tanker Ship Based on Experimentally Estimated Ultimate Strength. Polish Marit. Res. 26, 47–54. https://doi.org/10.2478/pomr-2019-0024

Woloszyk, K., Kahsin, M., Garbatov, Y., 2018. Numerical assessment of ultimate strength of severe corroded stiffened plates. Eng. Struct. 168, 346–354. https://doi.org/10.1016/j.engstruct.2018.04.085

Wu, C.-F., Hamada, M., 2009. Experiments : planning, analysis, and optimization. Wiley.

Xu, S., Zhang, H., Wang, Y., 2019a. Estimation of the properties of corroded steel plates exposed to salt-spray atmosphere. Corros. Eng. Sci. Technol. 54, 431–443. https://doi.org/10.1080/1478422X.2019.1613779

Xu, S., Zhang, Z., Li, R., Wang, H., 2019b. Effect of cleaned corrosion surface topography on mechanical properties of cold-formed thin-walled steel. Constr. Build. Mater. 222, 1–14. https://doi.org/10.1016/j.conbuildmat.2019.06.130

Zhang, W., Shang, D., Gu, X., 2006. Stress-strain relationship of corroded steel bars. Tongji Daxue Xuebao/Journal Tongji Univ. 34.